Supplementary Information

Crossover in the dynamics of cell wall growth controls *Caulobacter* division times

S. Banerjee, K. Lo, A. Selewa, T. Kuntz, M. Daddysman, A.R. Dinner and N.F. Scherer.

MATERIALS AND METHODS

Acquisition of Experimental Data. Data were acquired as in [1]. Briefly, the inducibly-sticky *Caulobacter crescentus* strain FC1428 was introduced into a microfluidic device and cells were incubated for one hour in the presence of the vanillate inducer. The device was placed inside a homemade acrylic microscope enclosure ($39'' \times 28'' \times 27''$) equilibrated to 31°C (temperature controller: CSC32J, Omega and heater fan: HGL419, Omega) and at other temperatures (see Supplementary Fig. 2). At the start of the experiment, complex medium (peptone-yeast extract; PYE) was infused through the channel at a constant flow rate of 7 μL/min using a synringe pump (PHD2000, Harvard Apparatus), which flushed out non-adherent cells. A microscope (Nikon Ti Eclipse with perfect focus system) and robotic XY stage (Prior Scientific ProScan III) under computerized control (LabView 8.6, National Instrument) were used to acquire phase-contrast images at a magnification of 250X (EMCCD, Andor iXon+ DU888 1k $\times$ 1k pixels; objective, Nikon Plan Fluor 100X oil objective plus 2.5X expander; lamp, Nikon C-HFGI) and a frame rate of 1 frame/min for 16 unique fields of view over 48 hours. In the main text we use a dataset consisting of 260 cells, corresponding to 9672 generations (division events) at 31°C.

Cell Shape Analysis. The acquired phase-contrast images were analyzed using a routine we developed (in Python) [1, 2]. Each image was processed with a pixel-based edge detection algorithm that applied a local smoothing filter, followed by a bottom-hat operation. The boundary of each cell was identified by thresholding the filtered image. A smoothing B-spline was interpolated through the boundary pixels to construct each cell contour. Each identified cell was then tracked over time to build a full time-trajectory. We chose to include only cells that divided for more than 10 generations in the analysis. A minimal amount of filtering was applied to each growth curve to remove spurious points (e.g., resulting from cells coming together and touching, or cells twisting out of plane). The timing of every division was manually checked, so the precision in determining this quantity results from the frame rate and not limitations of the automated analysis.

WGA Fluorescence Microfluidics Assay. To investigate the dynamics of cell wall growth over time in *Caulobacter crescentus*, we monitored the localization of fluorescent wheat germ agglutinin (flWGA) on the cell wall of the bacteria using the microfluidics platform we previously developed [1]. A 5 mL liquid culture of *C. crescentus* in PYE was prepared over night and diluted the following morning to an optical density at 660 nm of 0.1. Vanillate was added to this diluted culture at a final concentration of 0.5 mM to induce the production of the holdfast hfsA for 3 hrs. 1 mL of this culture was flowed into a cleaned microfluidics chip and allowed to incubate for 1 hr. A 20 mL syringe of PYE and a 3 mL syringe with 2 mL of PYE and 1 mL of flWGA were attached to two separate input ports into the microfluidics channel. Flow into the channel was resumed with media from the 3 mL syringe at a rate of 3.5 L/min for 15 minutes. Flow was then halted for 15 minutes to allow the cells to be covered with the flWGA. Media from the 20 mL syringe was flowed into the channel at a rate of 3.5 L/min. Image stacks with a 100 nm spacing were acquired (using MicroManager) at a position along the microfluidics channel with sufficient cell coverage every 10 minutes.

Deconvolution of Images. Captured images of an object (I) are a convolution of the actual object (f) and the point spread function (PSF) of the microscope (h):

$$I = \int_{-\infty}^{\infty} f(\vec{x})h(\vec{x} - \vec{x}')d^3\vec{x}' \ . \tag{S.1}$$

Given a measurement of the PSF and the acquired images of the object, deconvolution employs a classic maximum-likelihood estimation algorithm that calculates the most likely object to produce the acquired images [3]. This calculation is performed relatively quickly in the Fourier domain, where the integral (S.1) is transformed into simple multiplication in Fourier space. Deconvolution microscopy is widely used to remove the blurring imposed by the PSF of the microscope.

An image stack from each time point was deconvolved individually using commercial software (Huygens Deconvolution; Scientific Volume Imaging). Before performing the deconvolution, the 3D PSF of our oil immersion objective (Nikon), with a magnification of 100X and NA = 1.49, was measured by imaging static polystyrene beads with diameter of 100 nm coated with green fluorescent protein (Thermofisher). The PSF was sampled at 72 nm by 72 nm in the x-y plane and 50 nm in the z direction, thus satisfying the Nyquist criteria for our particular objective. Next, 17 image stacks corresponding to 17 time points were loaded into Huygens. Parameters such as background intensity, spatial sampling, objective NA, immersion index of refraction, and the signal-to-noise ratio (SNR) of objects were entered manually.

The background intensity was determined by calculating the mean intensity in an area of the image where there is no signal. The bacterial image stacks were sampled at 72 nm by 72 in the x-y plane and 100 nm in the z-direction. Because of photo-bleaching, the SNR of the bacteria will change as a function of time. At each time point, the SNR was calculated using the following equation: SNR $= \sqrt{N} = \sqrt{i_{\max}/i_{\text{single}}}$, where $i_{\max}$ is the maximum grayscale value of a pixel in the bacteria and i_{single} is the grayscale value due to a single photon incident on our detector. The value of i_{mean} is obtained at each time point from the measured images. The value of i_{single} is a calculated quantity using the parameters of our camera (Andor iXon EMCCD) such as quantum efficiency, A/D conversion, and system gain. A maximum number of 40 iterations was allowed for the deconvolution but Huygens reached a global minimum at ∼30 iterations for each time point.

Intensity uniformity index. A typical intensity profile at early times ($t < 50$ min) is spatially uniform around the cell center and then decays towards the poles. At later times, $t > 50$ min, the intensity profile is characterized by one minimum at the septum, given by $I_{\min}$, and two maxima at the stalked and the swarmer components, given by $I_{\max,1}$ and $I_{\max,2}$ respectively (Fig. 2C - inset). At each time point, we define the growth uniformity index for each intensity profile as, $D = 2I_{\min}/(I_{\max,1} + I_{\max,2})$. $I_{\min}$ is defined as the minimum in the intensity profile for $r - 2\sigma < x/l < r + 2\sigma$, where x is the coordinate along the centerline, r is the mean ratio of the daughter cell lengths, and σ is the standard deviation in daughter cell length ratio. Let $x_{\min}$ denote the location of $I_{\min}$ along the centerline coordinate. Then $I_{\max,1}$ is defined as the maximum in the intensity for $x < x_{\min}$ and $I_{\max,2}$ is the maximum in the intensity profile for $x > x_{\min}$. Thus, for $t \leq 50$, $I_{\min} \simeq I_{\max,1} \simeq I_{\max,2}$ and $D \simeq 1$. Whereas for $t \geq 50$ min, $I_{\min}$ represents the flWGA intensity value at the septum and is lower than both $I_{\max,1}$ and $I_{\max,2}$.

Size control models. The mixer model for size control (for $0 < t < \tau$) is defined by the following linear relationship between the size at birth, $l(0)$, and the size at division, $l(\tau)$,

$$l(\tau) = al(0) + \delta \, . \tag{S.2}$$

where τ is the division time. From this model, a sizer, a timer or an adder model can be recovered by considering appropriate limits for the slope and the intercept. A sizer is defined by $a = 0$, whereas an adder assumes a slope of unity, $a = 1$. In the timer limit we have $\delta = 0$.

From the plot of $l(\tau)$ vs $l(0)$ (Fig. 1B), we determine the parameters a and δ by a least-square linear fit to the scatter. For an adder model fit, we constrain the slope to unity and determine the added size, δ, from the intercept. Similarly, for the timer model fit, we determine the slope by assuming a zero intercept, as was done in Ref. [1]. To determine which of these models more

accurately represent our data, we evaluate the deviation of the models from the mean trend in our data. In particular we evaluate the following quantities:

$$\Delta_{\text{mixer}} = [al(0) + \delta] - \langle l(\tau) \rangle \ ,$$

$$\Delta_{\text{adder}} = [l(0) + \delta] - \langle l(\tau) \rangle \ ,$$

$$\Delta_{\text{timer}} = [al(0)] - \langle l(\tau) \rangle \ ,$$

where the angular brackets mean ensemble average. As shown in Supplementary Figure 1A, $|\Delta_{\text{mixer}}| < |\Delta_{\text{adder}}| < |\Delta_{\text{timer}}|$. For initial cell sizes close to the ensemble mean $\langle l(0) \rangle$, all the models converge to $\langle l(\tau) \rangle$.

From the best fit parameters, a and δ, we can predict the relationship between the added size and the initial size,

$$\Delta l = (a-1)l(0) + \delta \ ,$$

and also between $\kappa\tau$ and $l(0)$

$$\kappa\tau = \ln\left(a + \frac{\delta}{l(0)}\right) \ ,$$

without requiring any additional fitting parameters. (Fig. 1C,E). The corresponding deviations in Δl and $\kappa\tau$ from their mean values are given in Supplementary Figures 1 B,C.

Prior to the onset of constriction ($0 < t < t_c$), we use a pure timer model for size control, as evidenced by our data (Fig. 3). This is given by,

$$l(t_c) = a' l(0) \ , \tag{S.3}$$

where a' is determined by fitting a line of zero intercept to the scatter plot of $l(t_c)$ vs $l(0)$. As a result, κt_c is constant and has a value $\simeq \ln(a')$.

During cell-wall constriction phase ($t_c < t < \tau$), we use a pure adder model for size control, as evidenced by our data (Fig. 3). This is given by,

$$l(\tau) = l(t_c) + \delta' \ , \tag{S.4}$$

where δ' is determined by fitting a straight line of unit slope to the scatter plot of $l(\tau)$ vs $l(t_c)$. As a result, $\kappa(\tau - t_c)$ is negatively correlated with a value $\simeq \ln(1 + \delta'/l(t_c))$.

Crossover analysis from experimental data. To determine the crossover time, t_c, from the data on $w_{\min}$, we fit the following piecewise linear function to $\ln(w_{\min})$:

$$\ln(w_{\min}) = \begin{cases} at + b & \text{if } t < t_c' \\ b + (a-c)t_c' + ct_c' & \text{if } t \geq t_c' \,, \end{cases} \tag{S.5}$$

with four undetermined parameters a, b, c and t_c' obtained using the built-in FindFit function in Mathematica. A representative fit is shown in Supplementary Fig. 5A, where t_c' is the point of interesection of the two lines. We then compute the metric $Dw(t) = w_{\min}^i(t) - w_{\min}(t)$, where $w_{\min}^i = e^{at+b}$ (Supplementary Fig. 5B). Constriction is estimated to initiate when the metric Dw exceeds a threshold of 0.05 μm, which is equivalent to 1 image pixel. The crossover time, t_c, is taken to be 3 frames prior to the frame when Dw crosses the threshold value (Supplementary Fig. 5B), such that the determination of t_c remains robust to noise. We find the location for t_c is significantly spread out across generations when $w_{\min}(t)$ is plotted against absolute time (Supplementary Fig. 5C). When the constriction curves are aligned from the end of the cycle, as was done in Ref. [4], the individual curves collapsed much better, although the spread for t_c is significant (Supplementary Fig. 5D). By contrast, when the constriction curves are plotted against relative time, as shown in Fig. 3B, the locations of the crossover, t_c/τ, are much better aligned across generations (Supplementary Fig. 10).

Crossover point determination from septal growth model. To determine the crossover point in the analytical septal growth model, we implement the same procedure as performed for the experimental data. Specifically, we linearize the expression for $\ln(w_{\min}(t)/w_{\min}(0))$ around $\kappa t \sim \epsilon$, which gives us,

$$\ln(w_{\min}(t)/w_{\min}(0)) \sim \ln\left(\sqrt{-\mu + 2\mu e^{\epsilon} - \mu e^{2\epsilon} + 1}\right) + \frac{\mu e^{\epsilon}\left(e^{\epsilon}-1\right)(\kappa t - \epsilon)}{\mu - 2\mu e^{\epsilon} + \mu e^{2\epsilon} - 1} + \mathscr{O}[(\kappa t - \epsilon)^2] \,, \tag{S.6}$$

where $\mu = (l_0/w_{\min}(0))^2$. We then determine the point of intersection, κt_c of the above linear expression evaluated at $\epsilon \sim 0.05$ (near the start of cell cycle) and at $\epsilon \sim 0.56$, which corresponds to near the end of the cell cycle since $\langle \kappa\tau \rangle = 0.56$. The dependence of κt_c on $l_0/w_{\min}(0)$ is shown in Fig. 4B-inset.

Synchronized Cell Wall Growth Assay. This material is complementary to that presented in Fig. 2 of the main text. *C. crescentus* cells from the strain NA1000 were grown in 15 mL of M2X liquid culture media from 24 hours at 30°C to an optical density at 600 nm of 0.4. The swarmer cells from this liquid culture were isolated using a modified protocol [5, 6]. To summarize, the culture was spun at 6000 rpm for 20 minutes at 4°C. The pellet was then resuspended in 1 mL

of cold M2 media. The culture was then spun at 13000 rpm for 3 min at 4°C. The pellet was then resuspended in 900 μL of cold M2 media and 900 μL of Percoll. The culture was then spun at 11500 rpm for 20 min at 4°C, yielding two bands of cells. The upper band consisting of stalked cells was aspirated off, leaving the lower band of swarmer cells. The swarmer cells were then washed twice with 1 mL of M2 and spun at 11000 rpm for 3 min. The pellet was resuspended in 5 mL of M2X and 100 μL at a concentration of 1 mg/mL of fluorescent wheat germ agglutinin (flWGA), which had previously been shown to label the periphery of Gram-negative *E. coli* [7], was added to the resuspended culture and allowed to incubate with the cells for 10 min at 30°C to fully cover the cell wall. The culture was then diluted with 5 mL of M2X and grown in 30°C. 1 mL samples at 0, 20, 40, 60, 80, and 100 min were taken from the culture and frozen in dry ice. The cells were then fixed using 100 μL paraformaldehyde and washed with 100 μL phosphate buffered saline (PBS) and spun at 14000 rpm for 15 min. Microscope slides of the samples were made by combining 2 μL of sample, 2 μL of alginate, and 1 μL of 0.3 M Ca^{2+} to immobilize the cells. Fluorescence images of the cells in the slides were obtained through confocal fluorescence microscopy (Supplementary Fig 11A). The fluorescence data was obtained by using ImageJ by creating midline profiles of the cells and integrating the fluorescence intensity along the midline (Supplementary Fig. 11C). Supplementary Fig. 11A shows that the fluorescence intensity is spatially uniform prior to constriction (i.e., for samples at $t < 40$ min), but the flWGA intensity patterns exhibit a pronounced minimum at the septum where the cell-wall is invaginated ($t > 60$ min). Supplementary Fig. 11B presents deconvolution processed images obtained using the commercial software (Huygens). The deconvoluted single cell images more clearly show the diminished flWGA label in the septal region. Moreover, the 100 min image even hints at secondary invaginations in a predivisional cell, consistent with our previous report on intergenerational continuity [2]. Supplementary Fig. 11C shows the ensemble averaged normalized intensity profiles along the centerline axis of the cell at different time points. The spatial distribution of flWGA intensity suggests that growth is spatially uniform for $t < 40$ min and new cell-wall material is primarily synthesized at the invaginations for $t > 40$ min.

[1] S. Iyer-Biswas, C. S. Wright, J. T. Henry, K. Lo, S. Burov, Y. Lin, G. E. Crooks, S. Crosson, A. R. Dinner, and N. F. Scherer, Proceedings of the National Academy of Sciences **111**, 15912 (2014).

[2] C. S. Wright, S. Banerjee, S. Iyer-Biswas, S. Crosson, A. R. Dinner, and N. F. Scherer, Scientific Reports **5**, 9155 (2015).

[3] J.-B. Sibarita, in *Microscopy Techniques* (Springer, 2005) pp. 201–243.

[4] L. K. Harris and J. A. Theriot, Cell **165**, 1479 (2016).

[5] M. Evinger and N. Agabian, Proceedings of the National Academy of Sciences **76**, 175 (1979).

[6] M. E. Marks, C. M. Castro-Rojas, C. Teiling, L. Du, V. Kapatral, T. L. Walunas, and S. Crosson, Journal of Bacteriology **192**, 3678 (2010).

[7] T. S. Ursell, J. Nguyen, R. D. Monds, A. Colavin, G. Billings, N. Ouzounov, Z. Gitai, J. W. Shaevitz, and K. C. Huang, Proceedings of the National Academy of Sciences **111**, E1025 (2014).

[8] D. Ratkowsky, J. Olley, T. McMeekin, and A. Ball, Journal of Bacteriology **149**, 1 (1982).

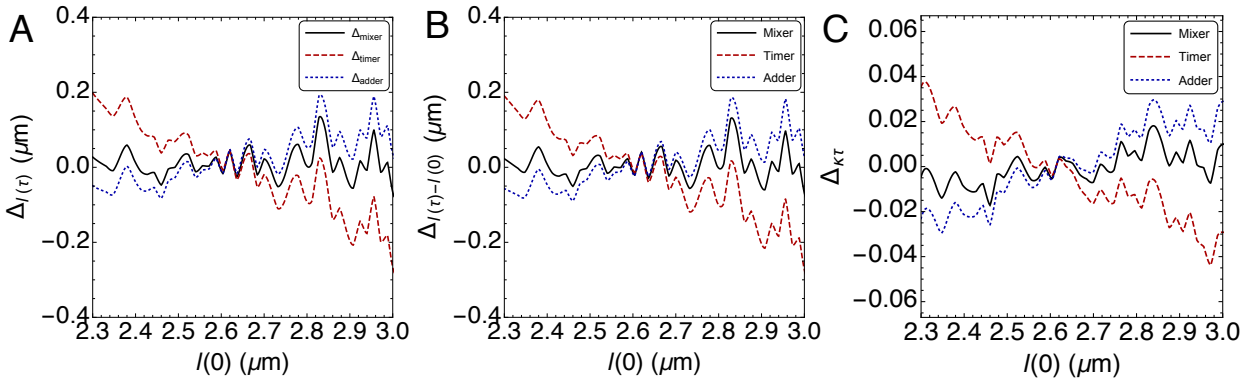

Supplementary Figure 1. **Errors in size control models**. Deviation about the mean for the (A) final length $l(\tau)$, (B) added length, $l(\tau) - l(0)$ and the (C) normalized cell cycle time, $\kappa\tau$, as given by a mixer (solid curve), adder (dotted curve) and a timer model (dashed curve).

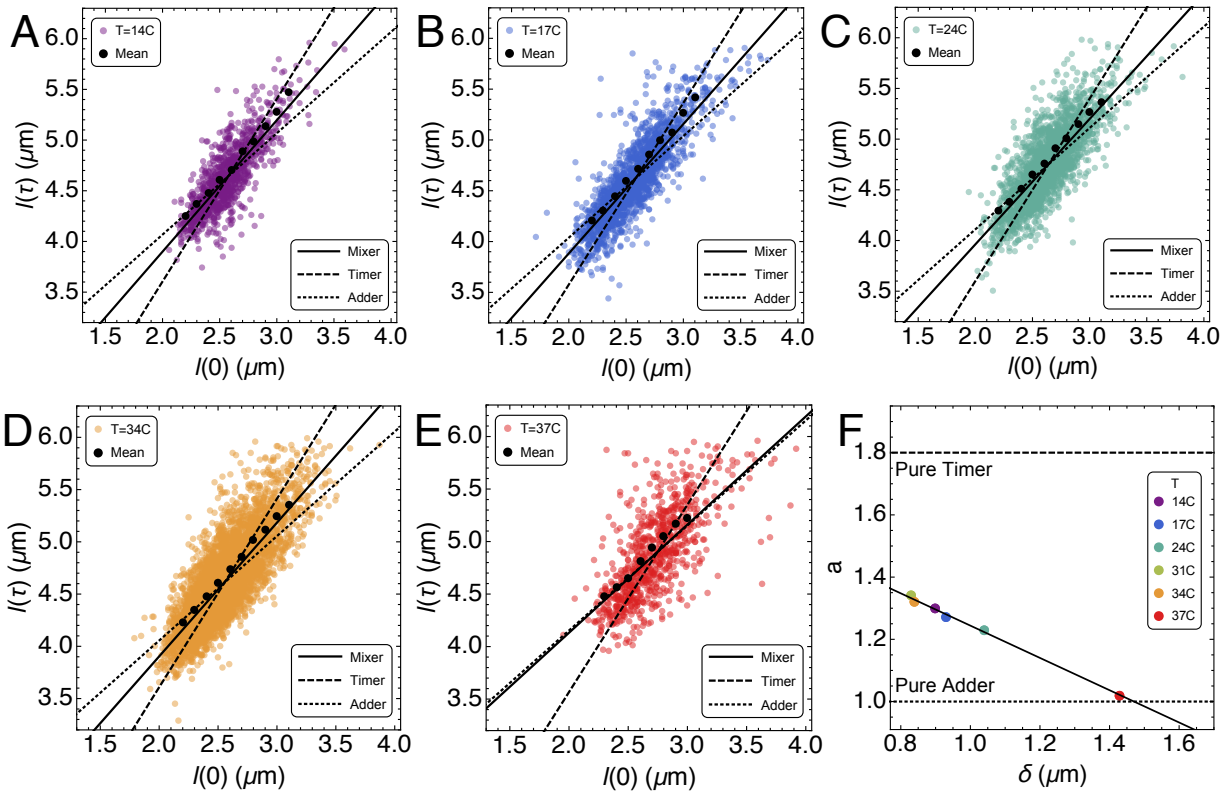

Supplementary Figure 2. **Cell size regulation at various temperatures.** (A-E) Correlation between the cell size at division, $l(\tau)$, and the cell size at birth, $l(0)$, at various temperatures. Black solid line represents a least square linear fit to the data (mixer model). Corresponding fits by timer and adder models are given by dashed and dotted lines, respectively. The solid circles represent mean data binned in $l(0)$. (F) Slope (a) and intercept (δ) of the mixer model, $A(\tau) = aA(0) + \delta$ where A is the cell area, as a function of temperature. With increasing temperature, cells approach the adder model of size control with $a \to 1$. Solid line is a least square linear fit, $a = -0.5\delta + 1.73$.

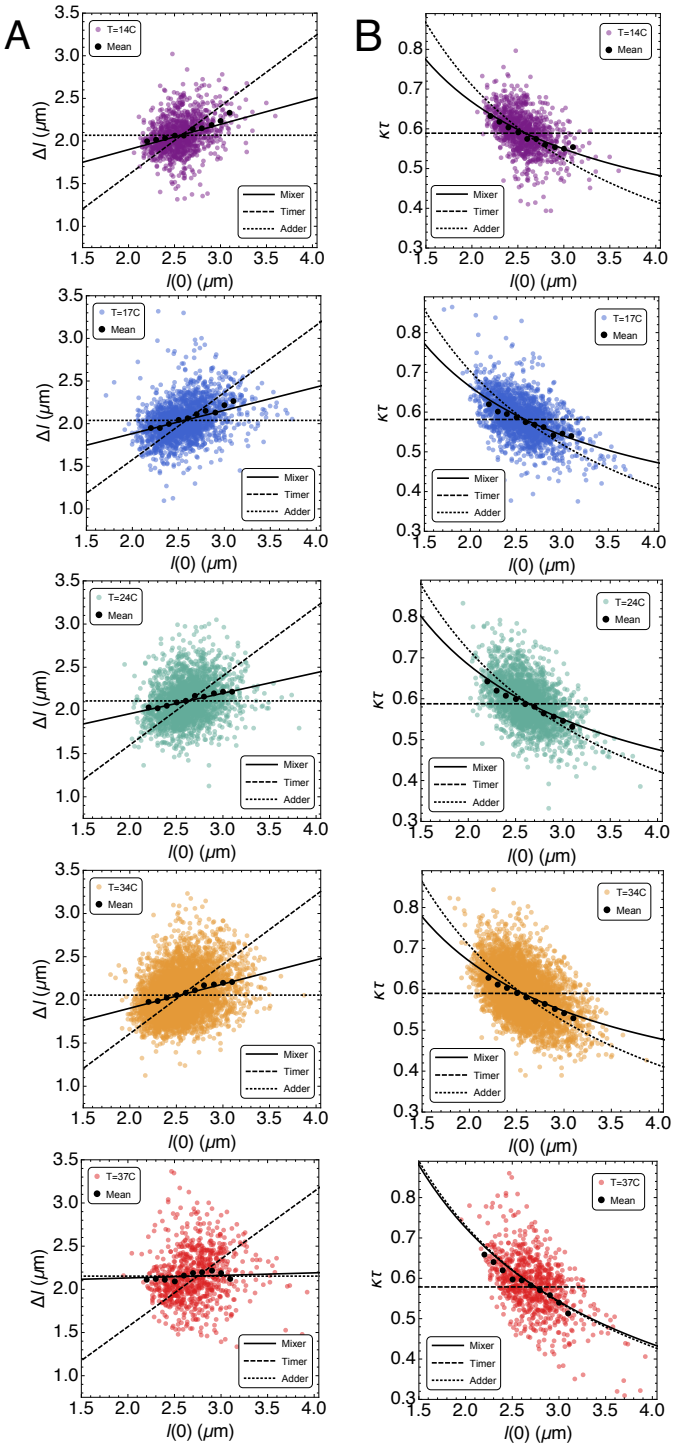

Supplementary Figure 3. **Control of added size and division times at various temperatures.** (A) Correlation between the added size, $\Delta l = l(\tau) - l(0)$, and the cell size at birth, $l(0)$, at various temperatures. (B) (Negative) Correlation between the normalized cell cycle duration, $\kappa\tau$), and the cell size at birth, $l(0)$, at various temperatures. Black solid line represents a least square linear fit to the corresponding data in Supplementary Fig. 1 (mixer model). Corresponding fits by timer and adder models are given by dashed and dotted lines. respectively. The solid circles represent mean data binned in $l(0)$.

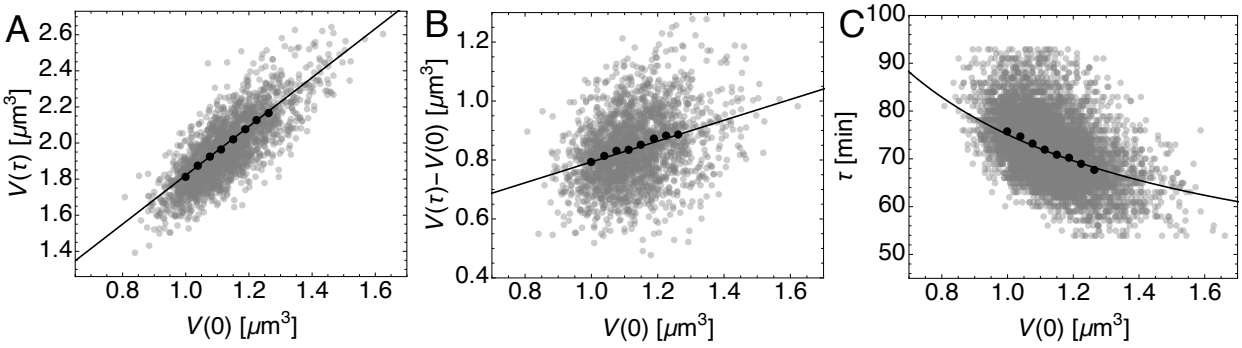

Supplementary Figure 4. **Volume data supports mixer model.** (A) Correlation between cell volume at birth and cell volume at division are supported by the mixer model: $V(\tau) = 1.35V(0) + 0.45$ (solid curve). Solid circles represent mean data binned in $V(0)$. Cell volume is estimated from measurements of cell midline length and width, assuming a circular cross-section. (B) Positive correlation between the added volume and the cell volume at birth. (C) Negative correlation between the division time and $V(0)$.

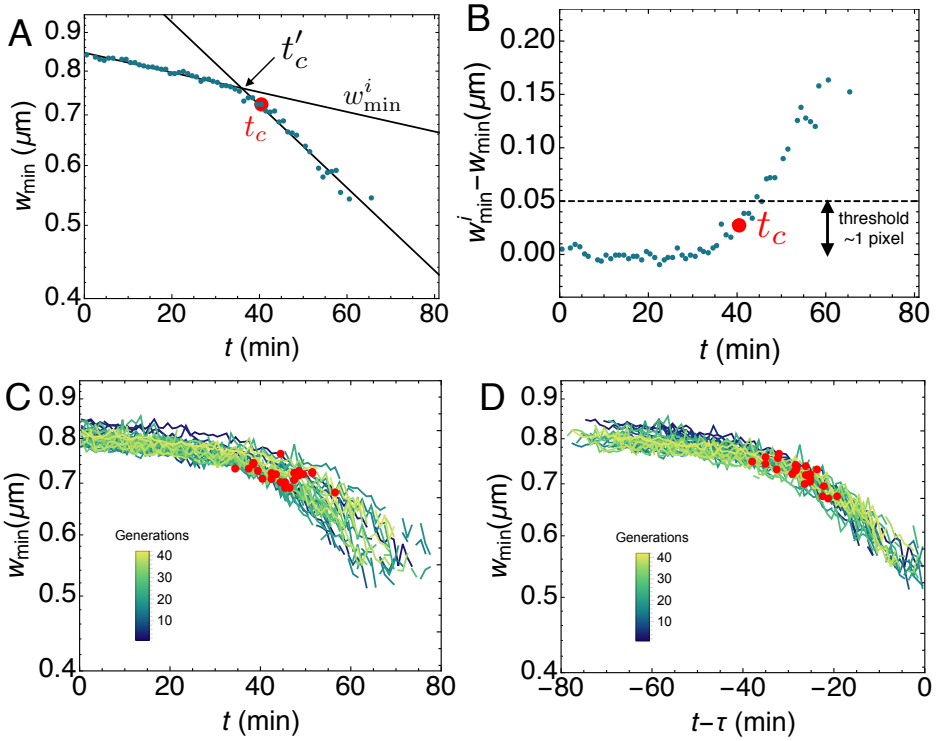

Supplementary Figure 5. **Determination of crossover time.** (A) Fitting the data for $w_{\min}$ with the piecewise exponential model in Eq. (S.5). Initial phase of decay is labeled $w^i_{\min}$ and the point of interesection occurs at t'_c. (B) Crossover time or constriction initiation time, t_c, is estimated to occur 3 frames prior to $w^i_{\min} - w_{\min}$ crossing the threshold 0.05 μm. (C) Dynamics of $w_{\min}$ vs t in semi-log scale. Red solid circles indicate crossover point t_c. (D) Dynamics of $w_{\min}$ vs $t - \tau$ in semi-log scale. Curves collapse although location of t_c is spread out.

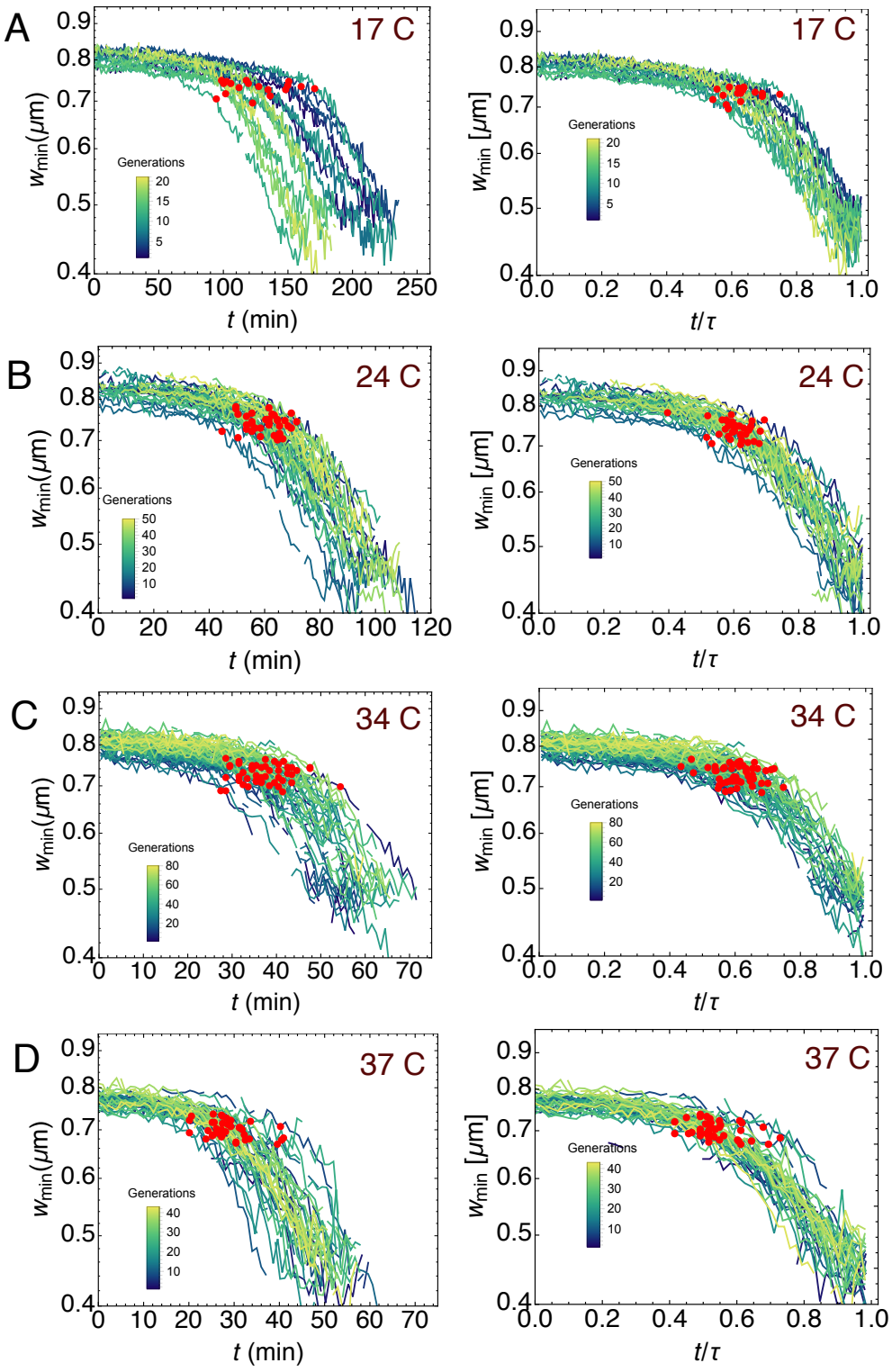

Supplementary Figure 6. **Crossover dynamics at various temperatures.** Dynamics of constriction ($w_{\min}(t)$) for a representative cell across all generations for temperatures equal to: (A) 17C (B) 24C (C) 34C and (D) 37C. Locations of the crossover (red) are much better aligned when the constriction curves are plotted vs relative time (right column) as opposed to absolute time (left column).

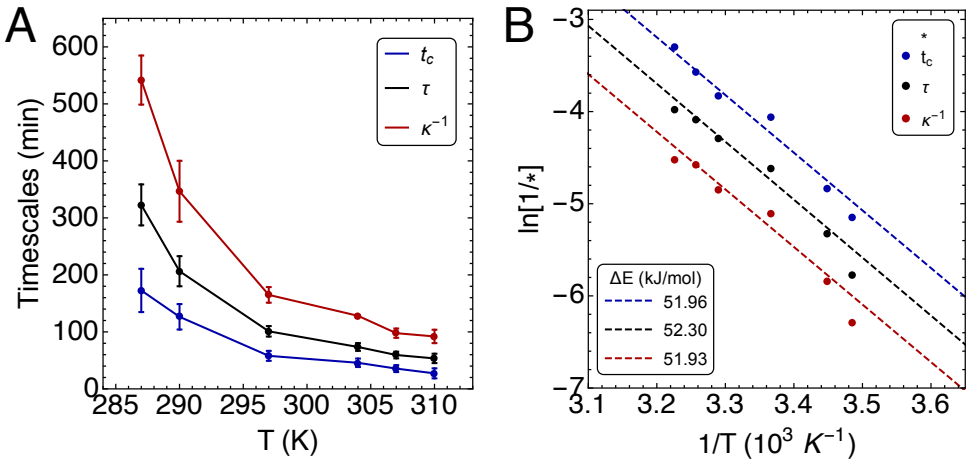

Supplementary Figure 7. **Temperature variations of the crossover time.** (A) The timescales t_c, τ and κ^{-1} monotonically decrease with increasing temperature. (B) Arrhenius plot for the variations of t_c, τ and κ^{-1} with temperature. We estimate the effective activation energy for crossing t_c to be approximately equal to the activation barrier for τ and κ^{-1}, $\Delta E \simeq 52$ kJ/mol. The estimate for ΔE comes from the slope of the dashed lines that are given by the Arrhenius equation: $\theta = \theta_0 e^{-\Delta E/k_B T}$, where θ represents κ, τ^{-1} and t_c^{-1}. We fit the Arrhenius equation in the temperature range: 14°C-37°C. The expected deviations from Arrhenius behavior are noticable at the extremes of the temperature range [8].

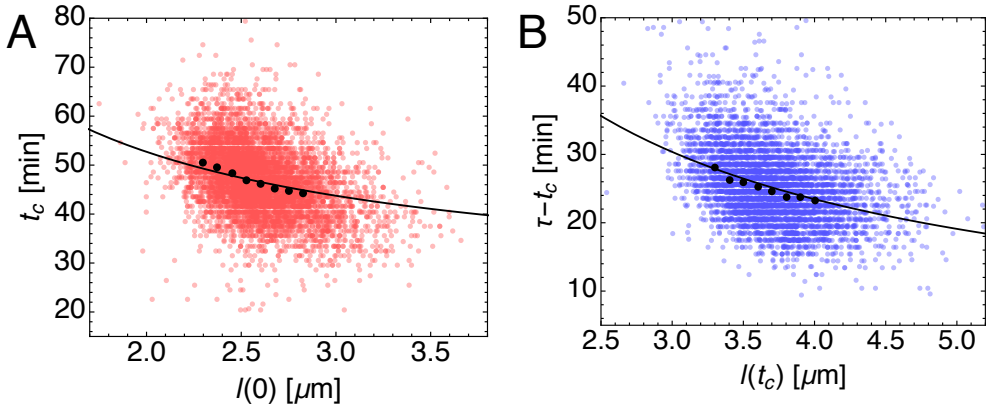

Supplementary Figure 8. **Preconstriction and post-constriction times are negatively correlated with cell size.** (A) Negative correlation between the crossover time and cell length at birth, consistent with a mixer model (solid curve). (B) Negative correlation between post-constriction time and cell length at t_c, consistent with a pure adder model (solid line). Solid circles represent mean data binned in cell length.

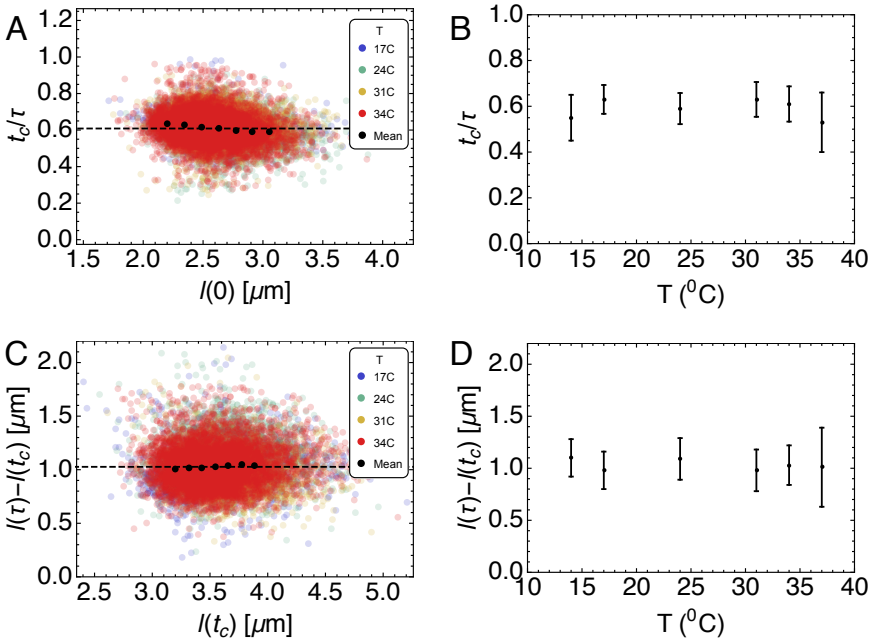

Supplementary Figure 9. **Relative timer to adder crossover at the onset of constriction at different temperatures.** (A) Relative crossover time, t_c/τ, is uncorrelated with the cell length at birth at all temperatures. Dashed line is the mean value for t_c/τ ($\simeq 0.6$) for all temperatures. (B) t_c/τ does not vary with changing temperature of the medium. Solid circles represent ensemblemean and error bars indicate ± 1 standard deviation. (C) Added length after constriction is uncorrelated with $l(t_c)$ at all temperatures, thus supporting a pure adder phase post constriction. Mean added size is 1.03 μm (Dashed line). (D) Post constriction added length does not vary with temperature. Solid circles represent ensemble mean and error bars indicate ± 1 standard deviation.

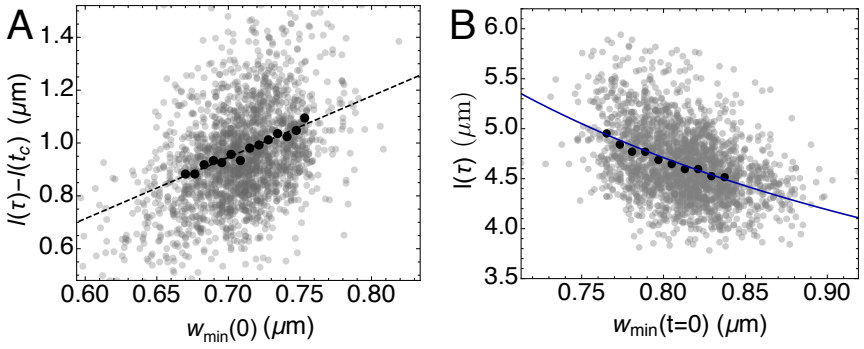

Supplementary Figure 10. **Cell shape controls cell size.** (A) Correlation between $l(\tau) - l(t_c)$ and the septal width $w_{\min}(t_c)$. The solid circles represent mean data binned in $w_{\min}(t_c)$ and the dashed line is a linear fit to the scatter. (B) Negative correlation between final cell size, $l(\tau)$, and the initial septal width, $w_{\min}(0)$. The binned data are in solid circles; whereas the prediction of the septal growth model, $l(\tau) = \delta \left(1 - \frac{a}{1+\Delta w_{\min}/l_0}\right)^{-1}$, is given by the solid line.

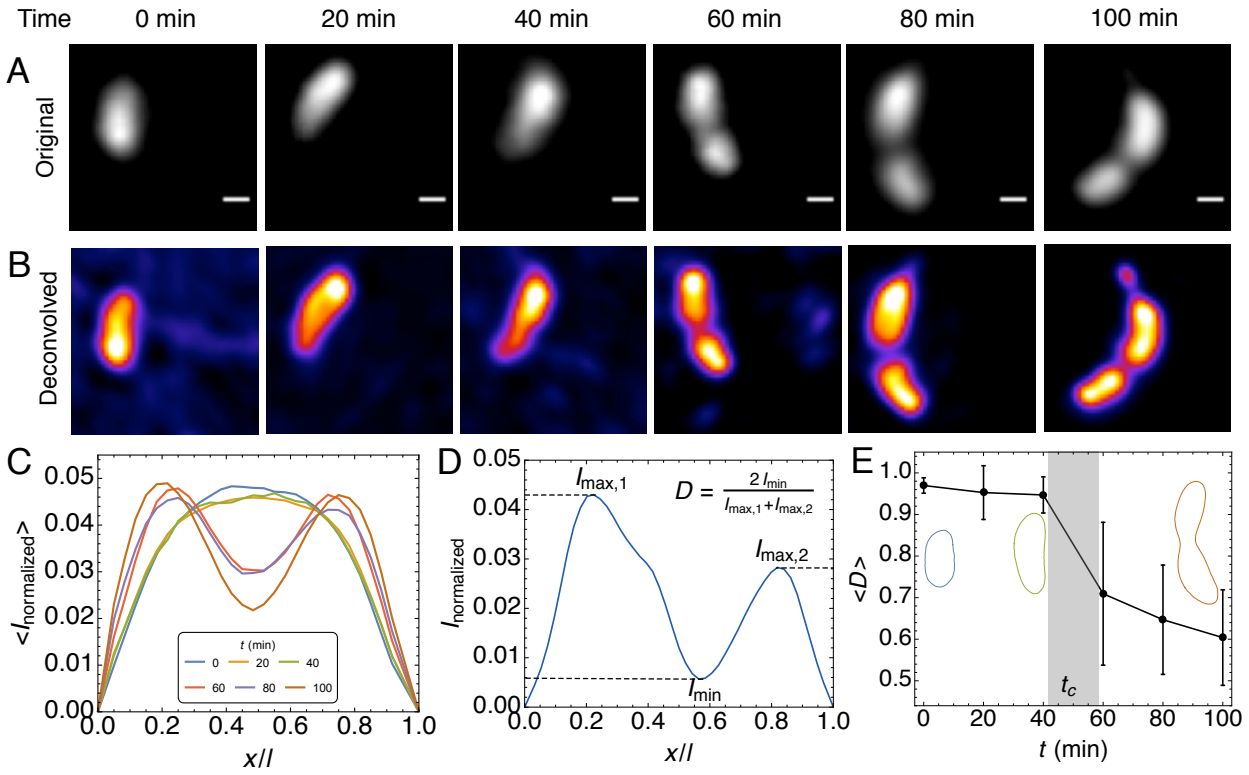

Supplementary Figure 11. **Crossover in cell wall growth dynamics at the onset of constriction**. (A) Confocal fluorescent images of *C. crescentus* cells labeled with fluorescent WGA taken after 0, 20, 40, 60, 80 and 100 min of growth in culture medium. The scale bars represent 0.5 μm. (B) Shows the same data but deconvoluted using the Huygens software package. The depletion of fluorescence reveals the underlying spatial pattern of growth, i.e. growth occurs where the fluorescence is minimized. (C) Ensemble averaged spatial distribution of normalized flWGA intensity along the centerline axis of the cell at t =0, 20, 40, 60, 80 and 100 min. The arc length along centerline, x, is normalized by the cell length, l. (D) A typical intensity profile is characterized by one minimum at the septum ($I_{\rm min}$) and two maxima near either pole ($I_{\rm max,1}$, $I_{\rm max,2}$). We define the index of uniformity of cell wall growth as, $D = 2I_{\rm min}/(I_{\rm max,1} + I_{\rm max,2})$. See Supplementary Information for more details. (E) Ensemble averaged dynamics of the growth uniformity index ($\langle D \rangle$) reveal a crossover from uniform growth ($\langle D \rangle \simeq 1$) to localized septal growth between 40 to 60 min (shaded area). Error bars indicate ± 1 standard deviation. The inset shows representative splined cell contours.